Optics Letters

Ultra-thin near infrared camera enabled by a flat multi-level diffractive lens

Sourangsu Banerji,[1] Monjurul Meem,[1] Apratim Majumder,[1] Fernando Vasquez Guevara,[2] Berardi Sensale-Rodriguez,[1] and Rajesh Menon[1,3,*]

[1]Department of Electrical and Computer Engineering, University of Utah, Salt Lake City, Utah 84112, USA
[2]Department of Mathematics, University of Utah, Salt Lake City, Utah 84112, USA
[3]Oblate Optics, Inc. San Diego, California 92130, USA
*Corresponding author: rmenon@eng.utah.edu

Received 30 August 2019; revised 16 September 2019; accepted 5 October 2019; posted 11 October 2019 (Doc. ID 376772); published 6 November 2019

We experimentally demonstrate a ∼1-mm-thick near infrared camera comprised of a multi-level diffractive lens coupled with a conventional monochrome image sensor. We performed careful measurements of the point-spread function, the modulation transfer function, focusing efficiency, aberrations, and the field of view of the camera.

https://doi.org/10.1364/OL.44.005450

Conventional cameras are comprised of multiple refractive lenses, primarily to correct for image aberrations. Each lens has to be manufactured separately, and then precise assembly is required to complete the camera. We have previously shown that a single multi-level diffractive lens (MDL), when appropriately designed, can correct image aberrations, thereby avoiding the assembly of multiple lenses [1]. Furthermore, by utilizing a small focal length for the MDL, it is possible to shrink the thickness of the camera. In this Letter, we designed and fabricated an MDL for the near infrared (NIR) ($\lambda = 850$ nm) with focal length $f = 1$ mm and diameter $D = 0.15$ mm and assembled it onto a monochrome complementary metal–oxide–semiconductor (CMOS) image sensor to form an ultra-thin NIR camera. The numerical aperture of this MDL is given by $\sin(\tan^{-1}(D/(2f))) = 0.075$. We also carefully characterized the performance of this camera in terms of its modulation transfer function (MTF), aberrations, and field of view.

Metalenses have been proposed as potential replacements for refractive lenses. However, we recently showed that MDLs not only are far easier to manufacture, but they also outperform metalenses for imaging [1]. We have previously demonstrated MDLs in the visible (450 nm–750 nm) [2,3], coupling two MDLs for magnification, [4], in the long-wave infrared (8 μm–12 μm), [5] in the short-wave infrared (875 nm–1675 nm), [6] and in the terahertz band (1 mm–3 mm) [7,8] and even shown the potential for almost unlimited bandwidth (2.5 μm–150 μm) [9]. In this Letter, we demonstrate an MDL with high efficiency at $\lambda = 850$ nm, utilizing relatively large microstructures (3 μm wide, 2.6 μm tall concentric rings) fabricated in a polymer film atop a glass wafer.

The MDL is modeled using scalar diffraction theory in the regime of Fresnel approximation [10]. The MDL is comprised of concentric rings of fixed width (3 μm) and heights determined by optimizing the focusing efficiency. The ring heights are constrained between 0 and 2.6 μm and allowed to occupy 100 discrete levels. A function was defined that computes the focusing efficiency for a given design. The focusing efficiency was defined as power within the focused spot [diameter of three times the full-width at half-maximum (FWHM)] divided by total incident power. By computing the gradient of this function with respect to the variable ring heights and applying a gradient-directed search, we are able to find the design that is able to maximize the focusing efficiency [1]. The optimized design is shown in Fig. 1(a). The device was fabricated in a photopolymer (S1813, Microchem) using grayscale optical lithography [9]. An optical micrograph of the fabricated device is shown in Fig. 1(b). The simulated and measured point-spread functions (PSFs) of the MDL are shown in Figs. 1(c) and 1(d), respectively. The PSF was measured by illuminating the MDL with collimated light from a supercontinuum source (SuperK Extreme, NKT Photonics) at $\lambda = 850$ nm (bandwidth ∼ 10 nm). The focal plane of the MDL was then magnified using an objective (RMS20X-PF, Thorlabs) and tube lens (ITL200, Thorlabs) and imaged onto a monochrome sensor (DMM 27UP031-ML, Imaging Source). The gap between the objective and tube lens was ∼90 mm and that of the sensor and the backside of the tube lens was ∼148 mm. The magnification of the objective–tube lens was 22.22×. This was necessary to capture the diffraction limited focal spot size at the focal plane with precision, as well as to measure the focusing efficiency. The simulated and measured FWHM were 5.97 μm and 5.64 μm, respectively. The efficiency was computed as the ratio of the sum of the intensity values in the sensor pixels within a circle of diameter equal to three times the FWHM to the sum of intensity values in sensor pixels within a circle representing the MDL aperture [1]. The simulated and measured focusing efficiencies were 94% and 92%, respectively.

We further measured the wavefront aberrations of the MDL using a Shack–Hartmann wavefront sensor. The aberrations are

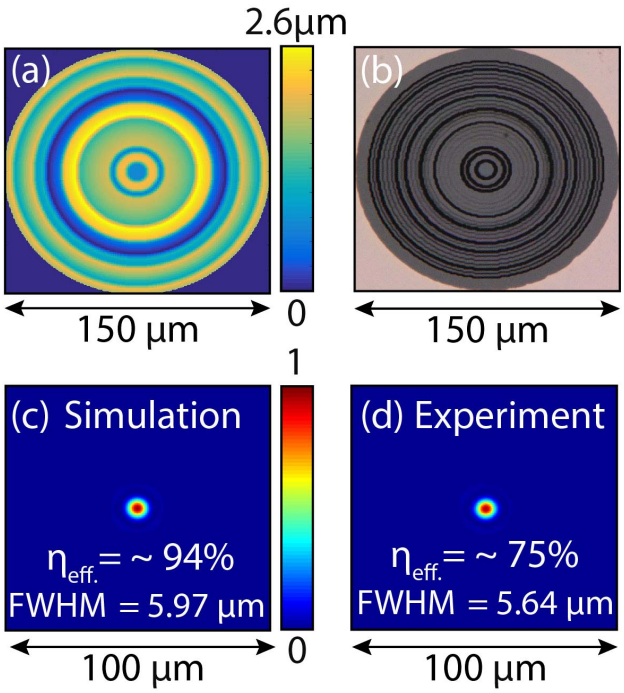

Fig. 1. (a) Designed geometry of the MDL and (b) optical micrograph of the fabricated device. (c) Simulated and (d) measured PSFs. The full-width at half-maximum (FWHM) and the focusing efficiency (η) are noted in the figures.

defined as the difference between the measured wavefront and the ideal spherical wavefront, and the difference is expressed as a linear sum of Zernike polynomials. The coefficients of the Zernike polynomials are illustrated in Fig. 2(b).

Next, we assembled a camera by placing the MDL in front of the same image sensor as for the PSF measurements [Fig. 3(a)]. Then, we captured still and video images of the Macbeth chart, as depicted in Fig. 3(b), the Air Force resolution target, as shown in Fig. 3(c), and a toy car, as seen in Fig. 3(d) (see Visualization 1). In each case, the exposure time was adjusted to ensure that the frames were not saturated. In addition, a dark frame was recorded and subtracted from the images. The resolution chart image shows that the resolved spatial frequency is ~145 line-pairs/mm. The field of view of the images taken with the MDL is about 50° × 40° in the horizontal

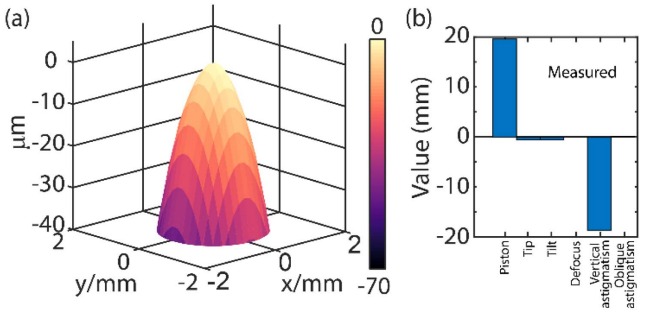

Fig. 2. (a) Measured wavefront of the MDL using a Shack–Hartmann wavefront sensor. (b) Measured coefficients of the constituent Zernike polynomials.

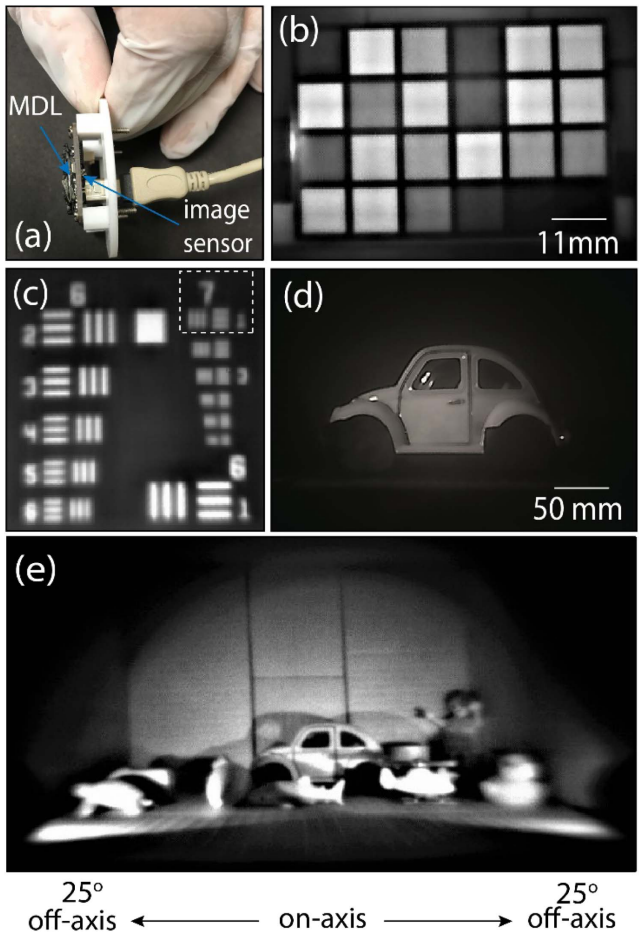

Fig. 3. (a) Photograph of the camera comprising a conventional image sensor and the MDL. Exemplary images taken with the camera of a (b) Macbeth chart, (c) USAF 1951 resolution chart, and (d) toy car (Visualization 1). (f) Image showing the field of view of the camera (approx. 50° × 40°). For (d) and (f), two NIR flashlights were used to uniformly illuminate the scene.

and vertical axes, respectively. In Fig. 3(e), we observe vignetting at the edges of the image. In the future, we can mitigate this by optimizing the MDL for both the on- and off-axis focusing. This, in principle, could open up the possibility of efficient wide-angle MDLs.

Next, we calculated the MTF of the MDL by taking the absolute value of the Fourier transform of the captured on-axis PSFs. The extracted MTF plots are shown in Fig. 4(a). The first

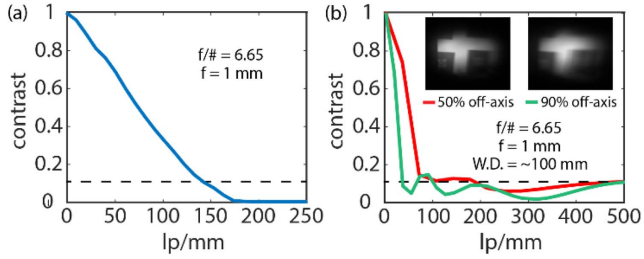

Fig. 4. Modulation transfer function (MTF) via (a) absolute value of the FFT of the measured PSF and via (b) the slanted-edge method for off-axis PSFs.

zero crossing of the on-axis MTF at 10% contrast occurs between 140 and 150 line-pairs/mm. This is also consistent with the resolution limits estimated from the chart in Fig. 3. For the off-axis PSF, we employed a slanted-edge method processed through open source software (MTFMapper) [11]. The object distance was ∼100 mm with the focused image formed at 1 mm behind the MDL. As seen from Fig. 4(b), the slanted-edge method was employed for two different conditions: namely, 50% off-axis and 90% off-axis. The MDLs highlight the first zero crossing of the on-axis MTF at 10% contrast at ∼80 lp/mm for the 50% off-axis condition. The basis for the 10% contrast is the fact that the human eye is relatively insensitive to detail at spatial frequencies where the MTF $\leq$ 10% [12].

In conclusion, the MDLs offer three main advantages: (1) the function of multiple conventional lenses may be achieved with one MDL, thereby reducing the need for precise alignment and reducing the number of optical elements in a camera; (2) short focal length MDLs are readily achievable, which allows for very thin cameras, as demonstrated in this Letter; (3) MDLs offer a drastic reduction in weight compared to conventional lenses, which is important for airborne and aerospace applications. By employing industry-standard lithography, it is possible to extend our current work to much higher numerical apertures (low f numbers) and enable ultra-thin microscope objective lenses as well as wide-angle camera lenses. In this Letter, we only demonstrated a fixed focus camera. In order to achieve variable focus, we will need to either incorporate multiple MDLs [4] or achieve focus tunability in each MDL itself.

Funding. Office of Naval Research (N66001-10-1-406); National Science Foundation (ECCS 1828480, ECCS 1936729).

Acknowledgment. We thank Brian Baker, Steve Pritchett, and Christian Bach for fabrication advice, and Tom Tiwald (Woollam) for measuring the dispersion of materials. We also acknowledge a grant of credit on Amazon AWS (051241749381) for computation. The support and resources from the Center for High Performance Computing at the University of Utah are also gratefully acknowledged.

Disclosures. Rajesh Menon is the founder of Oblate Optics, Inc., which is commercializing technology discussed in this Letter. The University of Utah has filed for patent protection for technology discussed in this Letter.

REFERENCES

1. S. Banerji, M. Meem, A. Majumder, F. G. Vasquez, B. Sensale-Rodriguez, and R. Menon, Optica **6**, 805 (2019).
2. P. Wang, N. Mohammad, and R. Menon, Sci. Rep. **6**, 21545 (2016).
3. N. Mohammad, M. Meem, B. Shen, P. Wang, and R. Menon, Sci. Rep. **8**, 2799 (2018).
4. M. Meem, A. Majumder, and R. Menon, Opt. Express **26**, 26866 (2018).
5. M. Meem, S. Banerji, A. Majumder, F. G. Vasquez, B. Sensale-Rodriguez, and R. Menon, "Broadband lightweight flat lenses for longwave-infrared imaging," arXiv: 1904.09011 (2019).
6. S. Banerji, M. Meem, A. Majumder, C. Dvonch, B. S. Rodriguez, and R. Menon, OSA Contin. **2**, 2968 (2019).
7. S. Banerji and B. Sensale-Rodriguez, Sci. Rep. **9**, 5801 (2019).
8. S. Banerji and B. Sensale-Rodriguez, Proc. SPIE **10982**, 109822X (2019).
9. S. Banerji, M. Meem, A. Majumder, B. Sensale-Rodriguez, and R. Menon, "Imaging over an unlimited bandwidth with a single diffractive surface," arXiv: 1907.06251 (2019).
10. M. Born and E. Wolf, *Principle of Optics*, 7th ed. (Cambridge University, 1999).
11. F. van den Bergh, J. Opt. Soc. Am. A **36**, 1126 (2019).
12. Imatest, "Sharpness: What is it and How it is Measured," 2019, http://www.imatest.com/docs/sharpness/.